

Mechanistic Study on the Gas-phase Ozonolysis of Isoprene and a Prediction of Hydroxyl Radical Yield

Luke Valin
Advising Professor Keith Kuwata
April 11, 2005

Abstract

Hydroxyl radical is a key atmospheric oxidant. Recent experiments and fieldwork have revealed the importance of alkene ozonolysis in forming hydroxyl radical. Isoprene (2-methyl-1,3-butadiene) is the most abundant atmospheric alkene. This study computes the isoprene-ozone potential energy surface with a high level ab initio and density functional theory composite method, CBS-QB3, predicts branching ratios using RRKM theory, and presents previously undiscovered dioxole chemistry elucidating possible stable products such as oxoepoxides and dicarbonyls. This study predicts a yield of 0.16 for hydroxyl radical and 0.23, 0.17, and 0.60 for methacrolein, methylvinylketone, and formaldehyde, respectively.

INTRODUCTION	3
A. Hydroxyl radical's atmospheric importance	3
B. Sources of OH radical	3
C. Faults of [OH] experimental analysis	5
D. Theoretical work on isoprene ozonolysis	5
E. Quantum Chemical Theories	6
F. Statistical Mechanical Theory	7
G. Isoprene Ozonolysis Overview	13
THEORETICAL METHODS	18
A. Quantum Chemical Methods	18
B. Statistical Mechanical Methods	19
RESULTS AND DISCUSSION	20
A. Overview	20
B. Differences in Treatment and Effects	21
C. Ozone Cycloaddition	22
D. Summary of Branching Ratios, Energetics, and Product Yields	23
E. Stable Product Comparison with Experiment and Previous Theoretical work	25
F. Theoretical discovery of oxo epoxides	28
G. OH yield prediction and analysis	28
H. Stabilized Criegee Intermediate Yields	32
I. Hydrogen-shift versus Dioxirane formation: Resonance Arguments	33
CONCLUSIONS	34
ACKNOWLEDGEMENTS	34
WORKS CITED	35
APPENDICES	39

Introduction

A. Hydroxyl radical's atmospheric importance

The hydroxyl radical is a key oxidant in the troposphere. Many natural atmospheric and anthropogenic species are controlled by the concentration of the hydroxyl radical. The hydroxyl radical's central importance in photochemical pathways is demonstrated in Figure 1.¹ Because of the hydroxyl radical's importance, current researchers are attempting to construct a general model to predict its concentration.

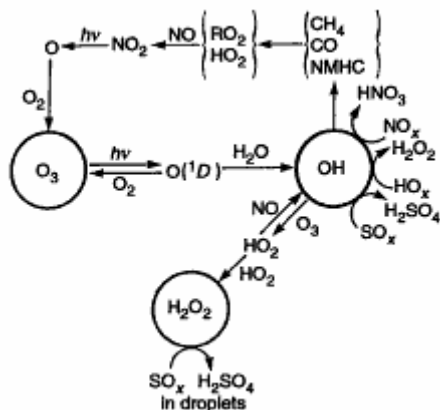


Figure 1. The central importance of OH as oxidizing agent in the atmosphere.¹

B. Sources of OH radical

Photochemical reactions involving ozone make up the major pathway of hydroxyl radical formation implying a strong daytime-dependence due to the necessity of light. Experimental data have shown that hydroxyl radical is present at nighttime implying the existence of non-light-dependent pathways.^{2,3} The experimentally suggested dark OH formation pathways involve ozone-alkene reactions. In Figure 2a, modeled and experimental hydroperoxy, hydroxy, alkoxy and alkylperoxy radicals (RO_x radicals) are compared considering only the light-dependent reactions while Figure 2b took both light-dependent and ozone-alkene reactions into the model's consideration.² When ozone-alkene reactions are ignored, the model predicts slightly lower concentrations than experimentally observed during daytime but grossly under predicts the nighttime

concentration. Strong model-experimental correlation is observed when ozone-alkene reactions are considered with a mid-day over prediction.

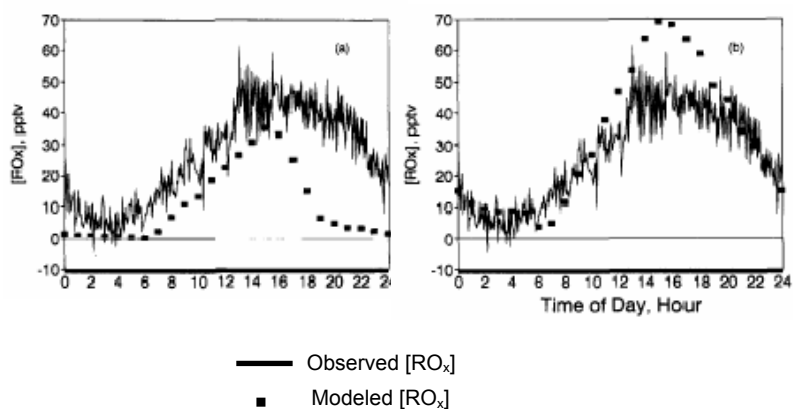


Figure 2.

Diurnal variation of RO_x radicals. $[RO_x]$ is expected to be similar in trend to $[OH]$. Measurements were made over one summer month of 1993 in Denver, Colorado. Especially cloudy conditions that month could lower the observed values during the daylight hours.²

Figure 3 is hydroxyl radical specific whereas Figure 2 took all RO_x radicals into account. Again, $h\nu$ -dependent formation predictions are short of the experimental measurement especially into the evening hours of the summer data and through the entire winter day.³

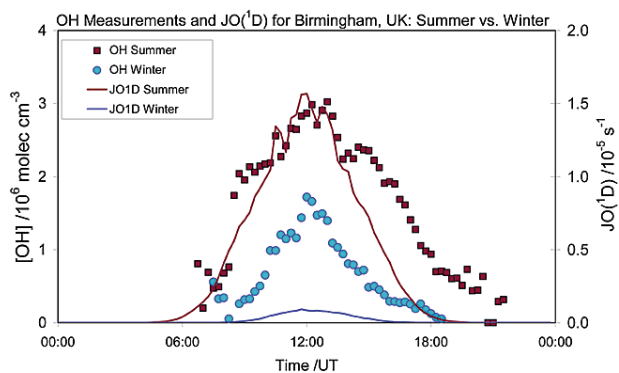


Figure 3.

Daytime variation of OH in the summer of 1999 and winter of 2000 at University of Birmingham, UK, compared to theoretical prediction with $J(O^1D)$, the rate of O_3 photolysis. Points represent a 15 minute time span, and concentrations are averaged over 14 days for summer and 11 days for winter.³

There are many biogenic and anthropogenic alkenes present in the troposphere with each one having a distinct reaction mechanism with ozone. In these early stages of investigation it is important to consider the major, natural, OH-forming alkene-ozone reactions for reasons of scale. Theoretical studies should focus on alkene-ozone reactions

that are known to produce hydroxyl radical and alkenes that have high atmospheric concentrations. Isoprene is naturally released by vegetation, and is the most abundant alkene in the troposphere.⁴ Isoprene has been shown to react with ozone to form OH. Furthermore, unusually high nighttime concentrations of OH radical have been reported above deciduous forests where isoprene is known to abound because of its biogenic origins.⁵

C. Faults of [OH] experimental analysis

Throughout the past decade, many experimental techniques have attempted to quantify OH formation from a variety of sources. However, OH's reactive nature makes it a highly problematic species to quantify even with modern techniques and tools including fluorescence assay by gas expansion (FAGE), laser-induced fluorescence (LIF), differential optical absorption spectroscopy (DOAS), chemical ionization mass spectrometry (CIMS), and ¹⁴CO oxidation.³ Low limits of detection are needed, $\sim 10^6$ molecules/cm³.³ Problems also arise in OH's tendency to react with reaction intermediates. With much work in improving the instrumentation for OH analysis, one σ uncertainties range from 7% up to 50% with most between 15% to 30%.³ Even with such uncertainty, experimental results for OH yield from the ozonolysis of isoprene show fair agreement. Eight reported values range from 0.19 to 0.53, with all but two results between 0.19 and 0.27.⁶ A fair variation in experimental results and the desire for a mechanistic understanding give importance to the creation of theoretical models.

D. Theoretical work on isoprene ozonolysis

i. Previous work and concerns

Recently, attempts have been made to map the potential energy surface (PES) of the ozone-isoprene reaction coordinate.^{6,7} The PES was described using CCSD(T) theory, an advancement of Hartree Fock (HF) theory, and corrected by a factor dependent on a density functional theory (DFT) method, B3LYP.⁶ With modern computing power,

we feel that CBS-QB3, a more accurate, costly composite method, can and should be employed for a system of this size.

Besides differing levels of theory, the previous model has left out consideration of a key, energetically favorable mechanistic intermediate, dioxole, and has also not allowed for the interconversion of the historical Criegee intermediates, a set of substituted carbonyl oxides resulting from the cycloreversion of a primary ozonide, which we show to be energetically feasible to some degree. The final key difference is a differing opinion on the fate of thermalized Criegee intermediates; the previous model believing a large fraction will form hydroxyl radical, and our model believing that moisture in the atmosphere will react with these intermediates and subsequently follow a non-OH-forming pathway.

ii. Important considerations in theoretical modeling

To adequately predict the percent yield of hydroxyl radical, it is important to consider two things. First, one must consider whether a pathway will lead to the formation of hydroxyl radical or not, and second, one must consider branching ratios of all mechanistic pathways. Branching ratios are calculated using RRKM theory with energetic and entropic information from quantum chemical calculations. In computationally exploring ozone-alkene reactions for OH production, it is important to fully characterize each transition state, each intermediate, and the feasibility of OH formation.

E. Quantum Chemical Theories

In general, quantum chemical methods are employed to determine relative energies. These methods are classified as ab initio, semi-empirical, or density functional theory (DFT). Ab initio methods are based on the first principles of quantum mechanics. Hartree Fock (HF) theory is the primary ab initio method and has become more accurate as it has been modified to better describe electron correlation, or how electrons interact with one another. DFT computes the electron density to determine energy inherently

treating electron correlation. Semi-empirical methods are based on certain predefined parameters for similar chemical systems and significantly cut computational costs and often accuracy.^{8 1995-96} This study exclusively uses ab initio and DFT methods.

F. Statistical Mechanical Theory

i. Overview

Branching ratios are calculated using statistical mechanics. Statistical mechanics is the study of energy, how it arranges itself, and how it transforms as it moves over a PES. With statistical mechanics, one is able to determine microcanonical rate constants, a means to determining the probability of formation of OH radical from a pathway. The energized intermediates of these low-pressure gas phase reactions are not at thermal equilibrium but are rather said to be energized to a shifted-thermal distribution and do not follow a Maxwell-Boltzmann distribution. Intermediates do not undergo collisional stabilization in the gas-phase fast enough to avoid further reaction. Statistical mechanics allows for the treatment of these energized species and the determination of microcanonical rate constants as a function of the internal energy and the molecular dispersal thereof.

ii. Potential Energy Surface (PES)

A PES describes the potential of a set number of atoms interacting over all space. This means that each particle can move in three directions. Each atom has three degrees of freedom (degrees of freedom). Therefore, a set of N atoms has $3N$ degrees of freedom. In terms of internal degrees of freedom, three degrees of freedom are subtracted because the set of atoms can move in any of the three dimensions. The same can be said for three rotational degrees of freedom unless linear arrangements where 2 degrees of freedom are identical and only two distinct degrees of freedom can be taken away. Therefore, we are left with $3N-6$ vibrational degrees of freedom or $3N-5$ if linear that describe atomic motion in relation to the other atoms and its effect on the potential energy. Therefore, minima in the PES are bound with respect to all vibrational degrees

of freedom. Transition structures, the barriers that connect minima, are first order saddle points meaning they have one less degree of freedom than minima and are bound in all vibrational degrees of freedom except for the one that is represented in the reaction coordinate.

iii. Extracting reaction coordinates from a PES

Representations of reaction coordinates can often be misleading because the transition structure is always represented as a hump (i.e., not being bound). In Figure 4,⁹ the familiar reaction coordinate is represented, but transition structures are also shown to be bound as they should be. It is important to remember that transition structures have real vibrational characteristics like minima. These ideas become important when considering how rate constants are calculated by considering both the vibrational states of the minima and transition structures.

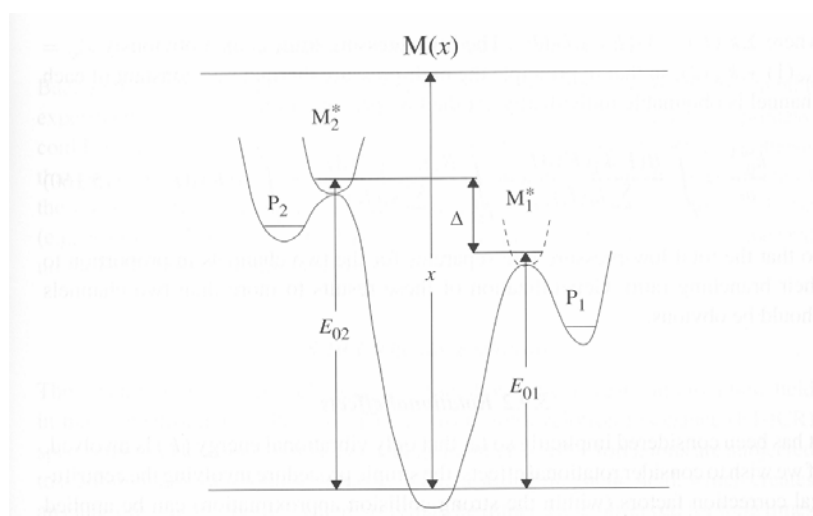


Figure 4. Depiction of an arbitrary reaction coordinate with a more theoretically accurate representation of the wells and first level transition structures.⁹

iv. RRKM theory and the Microcanonical Rate Constant, a Function of Energy

The microcanonical rate constants of competing reactions depend on the relative entropy of reaction barriers. Entropy is calculated as an increasing function of energy, so both a barrier's relative energy and entropy control the rate of reaction. Entropy of a transition structure is an increasing function of the energy above $v=0$. As an

intermediate's energy increases, there exist more rotational and vibrational states through which the intermediates can pass thus increasing the rate of reaction.

Equation 1 describes the microcanonical rate constant as a function of energy as it is employed in RRKM theory.¹⁰

$$k^i(E) = \frac{W_N^i(E-E_0^i)}{\rho_N(E)} \quad (1)$$

The numerator represents the sum of states of the transition structure between the $v=0$ state, E_0 and energy, E . The denominator tells the density of the intermediate's states as a function of energy. In simple terms, the numerator describes how 'wide' the barrier to reaction is while the denominator tells the degree of organization of the intermediate's energy.

v. Sources and Reservoirs of Internal Energy

RRKM theory and the Multiwell program suite treat all $3N-6$ vibrational degrees of freedom and one external rotational degree of freedom as capable of storing or exchanging internal energy. This idea comes from an assumption that non-linear polyatomic molecules rotate like a symmetric top and the largest two moments of inertia are approximately degenerate. The symmetric top axis, often called the K-rotor, is capable of exchanging energy with the internal vibrational modes while the two larger degenerate external rotations are considered to be inactive.¹¹

vi. Statistical Effects of the K-rotor

Since the K-rotor is assumed to exchange energy freely with internal degrees of freedom, it is important to consider how the moment of inertia, I , affects the rotational energy spacing. The rotational constant, B , is inversely proportional to the moment of inertia, I , as shown in equation 2.

$$B = \frac{h}{8\pi^2 c I} \quad (2)$$

If the K-rotor has a large moment of inertia, the rotational energy spacing should be small and have higher entropy. Structurally, more spherical molecules have a K-rotor with a larger moment of inertia whereas prolate molecules have a smaller K-rotor implying that a more spherical transition structure is entropically favored over a prolate transition structure.

vii. Calculating the Sum and Density of States

Sum and density of states are counted directly by a program, Densum, part of the Multiwell program suite, by considering all vibrational modes and the K-rotor.¹¹ Energy grain is defined as the interval at which states are counted and can affect the density of states calculation.

viii. Tracking Energy Distributions: Partitioning Energy upon Decomposition

Tracking the energy distributions of unimolecular reactions is not so difficult because unimolecular reactions do not involve the transfer of energy from vibrational modes to translational or rotational modes. Calculations can easily treat a unimolecular energy distribution and track its changes as reaction and parameterized collisional stabilization begin to compete. However, due to the nature of ozonolysis, this study must account for changes in the energy distribution when a product decomposes. The primary ozonide, an early ozonolysis intermediate, decomposes into two pieces allowing for vibrational energy to transfer to translational or rotational energy. In theory, the pieces can translate or rotate away from each other at any rate and still be able to maintain a conservation of momentum. Equation 3 describes how energy should be partitioned between two decomposing products.^{6,12,13}

$$f^D(E) = \frac{\rho_D(E)W_F(E^+ - E)}{\int_0^{E^+} \rho_D(\varepsilon)W_F(E^+ - \varepsilon)d\varepsilon} \quad (3)$$

D is the species of interest and this function describes its energy distribution. The numerator multiplies the density of states for D and the sum of states for F where E^+ is

the total available energy, which is determined by the reaction coordinate itself as described below. The denominator looks complex but is basically a normalizing factor.

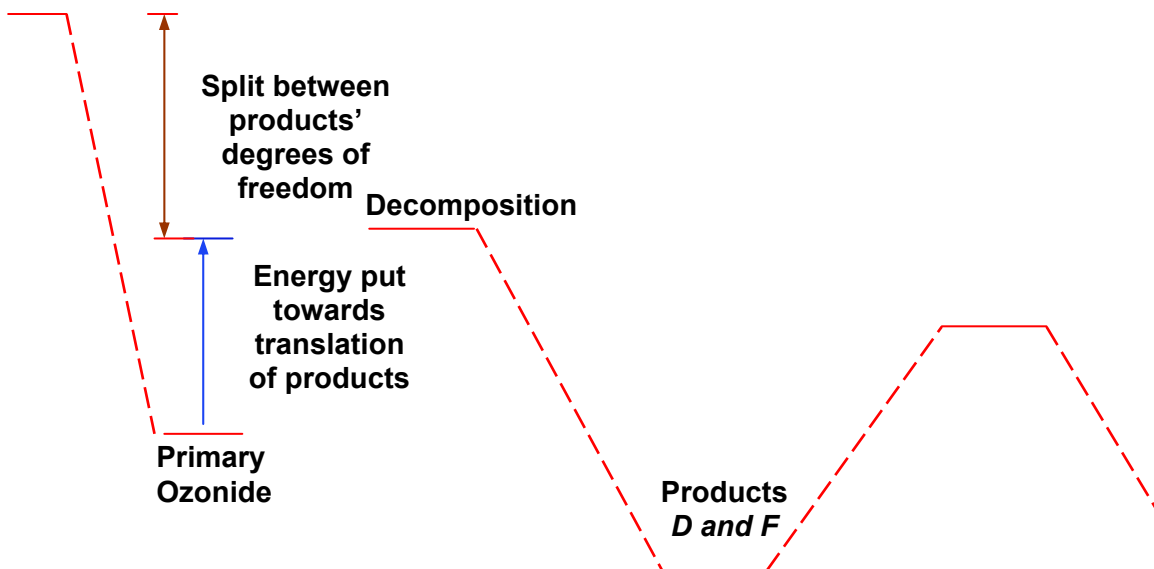


Figure 5.
An arbitrary reaction coordinate that helps explain equation five and the distribution of energy

The total available energy is theoretically considered to be the excess energy above the decomposition barrier seen visually in Figure 5.^{6,12} Energy below the decomposition barrier is thought to transform from vibrational energy to translational energy. Larger molecules receive more energy upon decomposition; energy is equally distributed amongst the products' degrees of freedom, which implies that larger molecules will receive more energy.

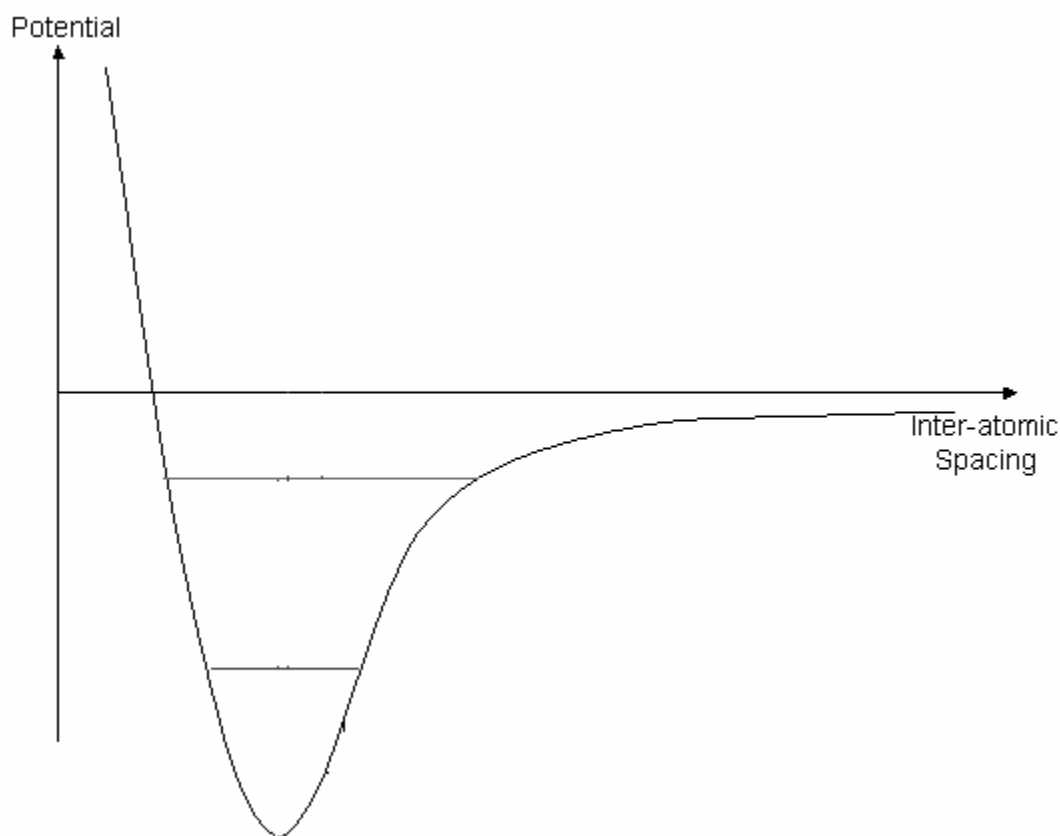
ix. Collisional Stabilization, the Biggest Theoretical Uncertainty

The largest theoretical uncertainty of this study arises from collisional stabilization. As the name collisional stabilization suggests, energy generally transfers from an activated species into the surrounding bath gas for probabilistic reasons. Each time a bath gas molecule interacts with an excited intermediate translational, rotational and vibrational energy modes are being engaged to different degrees making the determination of an average energy transfer per collision difficult. In the literature, this value varies over 1000% and is debated. Collisional stabilization also opens the

possibility for energy transfer between the vibrational modes of the excited species to its rotational and translational modes; a vibrational mode can propel or spin the excited molecule upon collision with a bath gas molecule.

x. Determining Collisional Frequency

In order to describe collisional frequency, pressure is the major factor, but the likelihood of collision is also determined by the attractiveness and distance of interaction for both bath gas and reaction intermediate. Lennard-Jones parameters are a simple description for these two parameters.¹⁴⁻¹⁶ Figure 6 graphically represents potential as a function of intermolecular distance. Lennard-Jones parameters represent the minimum of the energy curve, the depth being the 'attractiveness' or 'stickiness' and the distance being the radius of interaction.



As mentioned, pressure and temperature are most important to collisional frequency. Pressure and temperature vary over elevation, so it is important to consider the physical constitution of the troposphere. The troposphere varies between ~100 and 760 Torr from about 16 km of altitude to sea level, respectively. The temperature varies from ground temperatures to about -55 C°. Variation of chemical composition versus altitude is also important to consider for modeling the atmosphere, but not for this project.

xi. The Curtin-Hammett Principle

The Curtin-Hammett principle is specifically defined for a system at thermal equilibrium, but can be adapted to an activated system like the isoprene ozonolysis system. The Curtin-Hammett principle states that a system with two distinct conformers, each one having a distinct barrier to reaction and connected by an interconversion barrier, will undergo reaction as if there were only one minimum and two exit barriers so long as the barrier to interconversion is much lower than the barriers to reaction. Invocation of the Curtin-Hammett principle assumes that only the free energy of the reaction barriers and the lowest energy conformer are important for determining rates.

G. Isoprene Ozonolysis Overview

The mechanism being explored is a set of unimolecular reaction pathways after the ozonolysis of isoprene graphically displayed in Figure 7. Bimolecular reactions are not considered because intermediates of isoprene ozonolysis are chemically activated and unimolecular reaction will occur before two reactive species collide. Isoprene is a conjugated diene with its 1,2 alkene having a higher degree of substitution. The electron donating characteristics of the substituted methyl group make the 1,2 alkene more likely to undergo ozone cycloaddition. The ratio of addition at the 1,2 alkene versus the 3,4 alkene is theoretically reported to be 59% and 41% respectively.⁶ Cycloaddition at the 1,2 alkene is believed to be the only pathway leading to OH formation. Ozone cycloaddition results in the formation of a primary ozonide, a chemically activated

intermediate that immediately undergoes cycloreversion forming a carbonyl and a carbonyl oxide. For each primary ozonide, two classes of cycloreversion exist. Therefore, at this point in the mechanism, there are four possible product sets due to two possible cycloaddition pathways and two possible cycloreversion pathways for each of the primary ozonides: methacrolein (MACR) and formyl oxide, methacrolein oxide (MACRox) and formaldehyde, methylvinyl ketone (MVK) and formyl oxide, or methylvinyl ketone oxide (MVKox) and formaldehyde. MVK and MVKox are derived from the ozonolysis of the 1,2 alkene whereas MACR and MACRox result from ozonolysis of the 3,4 alkene. Carbonyl oxides are a chemically activated species that undergo one of three competing mechanistic pathways: hydrogen shift (source of OH radical), dioxirane formation (not an OH source), or dioxole formation (not an OH source). Formyl oxide is known to produce OH radical, but its cause and quantity are currently being widely debated in the literature, so for now, this species will be left untreated assuming its impact to be fairly minor. There are four conformers of both MACRox and MVKox with high energy barriers between the cis and trans vinyl carbonyl oxides due to the necessity to break π -bonding for rotation to occur. Because the barriers to conversion to other conformers and to reaction are of similar magnitude, the fate of the pathway is complex and needs RRKM theory to determine the branching ratios.

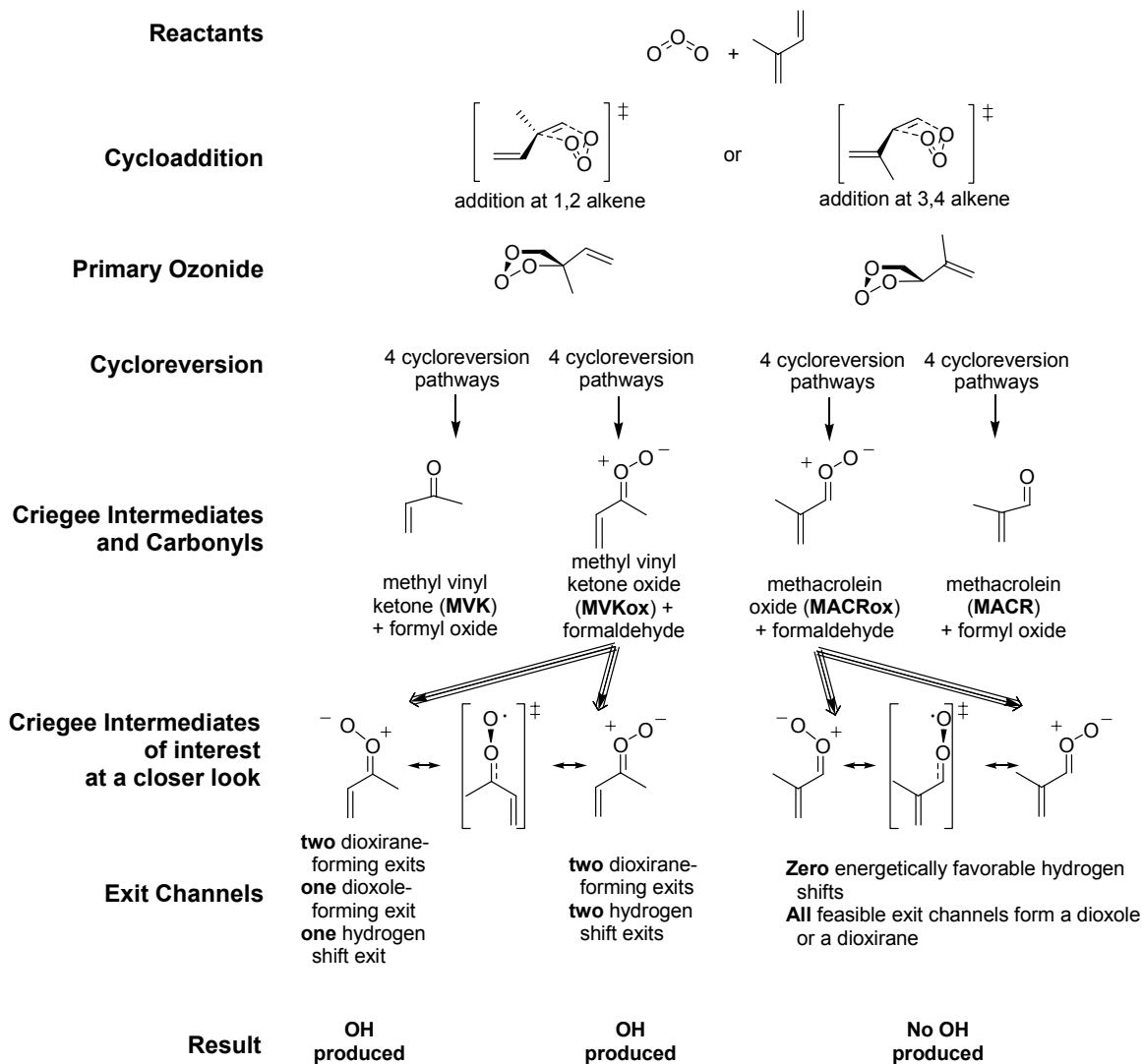
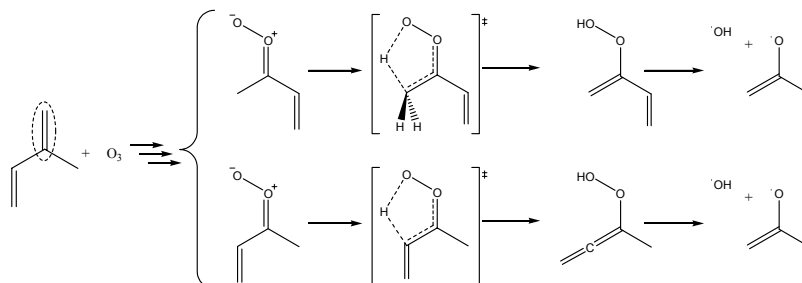


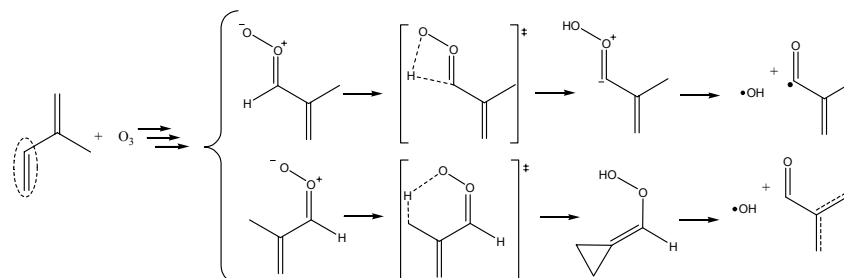
Figure 7. Summary of reaction pathways resulting from isoprene ozonolysis. The most important OH source from these mechanisms is believed to come when there is an available hydrogen atom in the alpha position to the carbonyl oxide as in Scheme 1.⁷



Scheme 1. Two of three possible hydrogen-shift reactions resulting from ozonolysis of the 1,2 alkene of isoprene.

In the literature, abstraction of the allylic hydrogen is energetically favored to abstraction of the vinylic hydrogen, and is thus a more important source of OH radical.⁷ These intermediates arise only from the ozonolysis of the 1,2 alkene of isoprene. For the top reaction schematic in Scheme 1, rotation of the vinyl group has no effect on the accessibility of hydrogen atoms; therefore, hydrogen-shift is possible. For the bottom reaction shown in Scheme 1, rotation of the vinyl group removes the chance for hydrogen abstraction; the barrier for 1,5 hydrogen shift leading to carbene formation has not been reported in the literature.

Previous studies have ruled out the importance of a 1,3 acyl hydrogen shift or 1,5 hydrogen shift described in Scheme 2.⁷

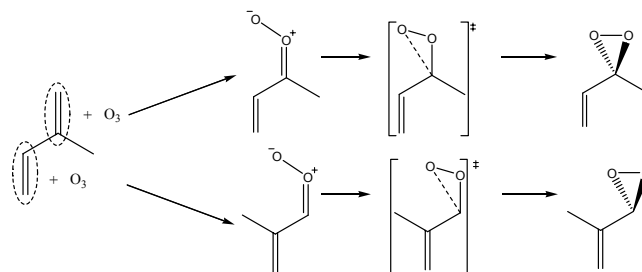


Scheme 2.

Two of three possible hydrogen-shift reactions resulting from the ozonolysis of the 3,4 alkene of isoprene

While these pathways are considered unlikely we will still investigate their possibility with the enhanced level of theory. For the top scheme, rotation of the vinyl group has little impact, but for the second conformer, vinyl rotation removes any chance for hydrogen shift.

Closure to dioxirane has previously been reported as the main competition to hydrogen-shift. Scheme 3 demonstrates dioxirane closure.

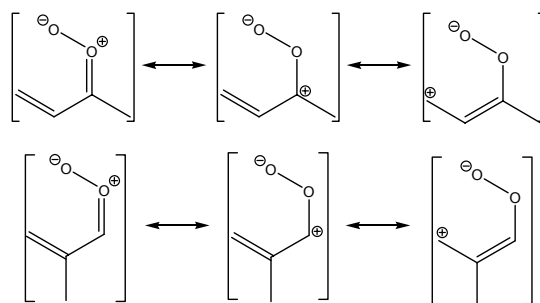


Scheme 3.

Two of a possible eight dioxirane closure reactions resulting from the ozonolysis of either alkene of isoprene

Closure to dioxirane is possible from all MVKox conformers and MACRox conformers while only one for each is depicted above; rotation of the oxide group or vinyl group makes no large electronic difference to the reaction scheme. Dioxirane closure has previously been shown to be slightly less competitive than hydrogen shift for the syn-methyl conformers.⁷

Previously, dioxirane formation was considered the only exit channel for MACRox because of the high energy for 1,3 acyl hydrogen shift barrier.⁷ Now, based on electronic arguments, a dioxole-forming channel is thought to exist. In Scheme 4, resonance contributors give logical explanation to the dioxirane closure but additionally justify the formation of a five-membered dioxole ring.

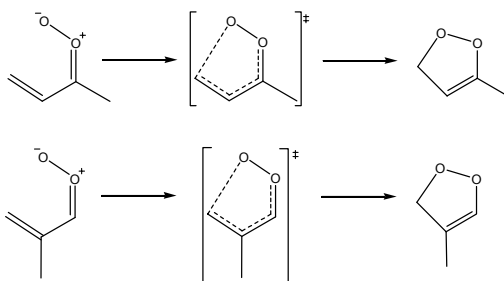


Scheme 4.

Three major resonance contributors for closed shell MVKox and MACRox. Carbocationic character implies two ring closing reactivities.

While the secondary or tertiary stabilized carbocation responsible for dioxirane reactivity is a more important resonance contributor than the primary carbocationic contributor responsible for dioxole formation, the overriding factor affecting reaction will be the

difference in ring strain. Dioxole's five-membered transition structure shown in Scheme 5 should be favored.



Scheme 5.

Dioxole formation is believed to occur from only one conformer of both MVKox and MACRox with the oxide and vinyl groups in proximity.

Theoretical Methods

A. Quantum Chemical Methods

All quantum mechanical calculations were performed in the Gaussian 03 program suite. Since the system is being defined with a highly accurate method, the costs are also high. In order to cut computational costs, geometry optimizations were run using B3LYP DFT^{17,18} and the 6-31G(d,p) basis set.^{19,20} The PES was further described when harmonic vibrational frequencies were calculated. From these data, each reported minimum was shown to have all real frequencies and that each transition structure had only one imaginary frequency. In a piece of the Gaussian software suite, a visualization program, Gaussview, allows for the animation of the calculated vibrational frequencies and when the animation was unclear intrinsic reaction coordinate (IRC) calculations^{21,22} were performed to clarify so that a TS was properly described for the minima it connected.

B3LYP is a low-cost, fairly accurate DFT method for the medium-sized organic systems we are investigating. It has been widely used to describe the oxidation reactions in the atmosphere.^{6,7,23-28} B3LYP has a tendency to under predict the relative energies of hydrogen-shift transition barriers.^{26,29-34}

Because OH production from the ozonolysis of isoprene depends so heavily on the relative energy of hydrogen-shift barriers, the PES was determined with the CBS-

QB3 composite-method model of Petersson and co-workers³⁵, which has recently been shown to have better agreement with experimentally-determined energy barriers.^{29,36-39} The idea behind CBS-QB3 composite method is the desire to most accurately represent the Schrödinger equation while maintaining a low cost. The Schrödinger equation is solved at an infinite basis set and an infinite level of treating electron correlation. Unfortunately, at this high level of theory and basis set, cost is infinite. CBS-QB3 determines energies at a high level of theory and small basis set, a medium level of theory and a medium-sized basis set, and at a low level of theory and an extrapolated infinite basis set.^{8 1995-96} The results are weighted and combined so that they best fit with experiment according to Petersson and Coworkers.³⁵ CBS-QB3 optimizes geometries at the B3LYP/6-311G(2d,d,p) level, giving more polarization functions than the 6-31G(d,p) basis set discussed earlier, uses CCSD(T)/6-31G(d')^{40,41} as the highest level treatment of electron correlation and smallest basis set, and extrapolates to a complete basis set at the MP2 level of theory, which is one step up in the treatment of electron correlation from HF or the minimum level of treatment.

B. Statistical Mechanical Methods

Statistical mechanical methods were performed by Barker's Multiwell program suite.^{42,43} Relative energies corrected to the $v=0$ vibrational level were determined the quantum mechanics CBS-QB3 calculations. Structure and structural characteristics such as harmonic vibrational frequencies and moments of inertia were determined in the B3LYP/6-311G(2d,d,p) step of the CBS-QB3 calculations. The microcanonical rate constants, $k(E)$, were determined using Rice-Ramsperger-Kassel-Marcus (RRKM) theory. RRKM theory is equivalent to conventional transition state theory but is different in that it calculates the microcanonical rate constants, a function of intramolecular energy, whereas transition state theory calculates the canonical rate constant, a function of temperature.⁴⁴

As mentioned earlier, theoretical assumptions need to be made in order to run statistical mechanics RRKM calculations on our particular system. Assumptions made affect collisional frequency, collisional stabilization, and energy partitioning. For collisional frequency, we have assumed N₂ as the bath gas at 298 K within the 0-760 Torr range, and selected Lennard-Jones (LJ) Parameters for N₂ of $\sigma=3.74 \text{ \AA}$ and $\epsilon=82 \text{ K}$.^{14,15} No LJ parameters for a species of satisfactory resemblance to our species of interest had been determined in the literature, so a chemical engineering method using a group additivity scheme was used to approximate. To estimate the LJ parameters of MVKox, methyl acrylate was used because no data exist for the oxide functional group; the parameters are $\sigma=6.29 \text{ \AA}$ and $\epsilon=358 \text{ K}$.^{16,45,46} The primary ozonide's LJ parameters were determined by the same scheme, and determined to be $\sigma=7.84 \text{ \AA}$ and $\epsilon=620 \text{ K}$.⁴⁶⁻⁴⁸

To estimate the effects of collisional stabilization, the exponential-down model was employed and the average energy transferred per collision ($\langle E_d \rangle$) was set to 300 cm^{-1} .^{43,49} This value is typical for a system of this type.

$$e^{-\frac{|E'-E|}{\alpha(E')}} , \text{ for } E' > E$$

The expression above represents the exponential-down model; it represents the energy that will be collisionally deactivated each occurrence. The denominator is the assumed average $\langle E_d \rangle$ value. E' is the molecule's energy before collision and E is after. As the collisional deactivation energy gets far away from $\langle E_d \rangle$, its occurrence exponentially decreases.

RRKM theory is used to calculate the microcanonical rate constants that are so important in comparing competing reactions.

Results and Discussion

A. Overview

This report contains the bond length characterization (appendices A1-13), CBS-QB3 electronic energy plus zero-point energy characterization for each of the minima and first-order saddle points (transition structures) on the isoprene ozonolysis PES from the quantum chemical calculations. Energies are reported with respect to the energy of the lowest energy Criegee intermediate. Branching ratios reported come from solutions to master equation simulations and RRKM theory.

B. Differences in Treatment and Effects

In comparing results from this study with the results of the previous theoretical analysis of isoprene ozonolysis, it is important to consider the differences in treatment. Energetically the reactants' energy and cycloaddition barriers are higher, cycloreversion barriers are lower, and minima and exit barriers are fairly similar to those of the previous study. This study predicts ~8-10 kcal/mole greater activation for both MACRox and MVKox because of higher cycloaddition barriers and lower cycloreversion barriers as can be seen with regards to the theory in Figure 5. The dioxole pathway opens a lower energy exit channel from conformers CI 1c,d and 3c,d. The Curtin-Hammett principle is not invoked in the CI interconversion and exit channel step in this study meaning that conformer interconversion is fully treated. This study's average collisional stabilization energy $\langle\Delta E\rangle$ is 300 cm^{-1} per collision while the previous study uses a slightly lower value of 250 cm^{-1} per collision. An energy grain of 10 cm^{-1} is used in this study while the past study uses a value of 100 cm^{-1} .

These small modifications in the procedure could affect the results. Criegee Intermediates in this study are more vibrationally activated, which could lead to a greater chance of reaction and a lesser chance of stabilization. The dioxole forming channel decreases the importance of dioxirane exits from CI 1c 1d, 3c, and 3d and increases the chance of reaction over stabilization for conformers CI 1 and 3 c,d. By not invoking the Curtin-Hammett principle in the Criegee Intermediate interconversion and reaction step,

product yields may vary slightly and the probability of collisional stabilization may be greater as passing through interconversion barriers may take more time. Increases in the $\langle \Delta E \rangle$ value slightly increases the probability of collisional stabilization as each collision will drain away more energy on average. The smaller energy grain better represents the sum and densities of states.

C. Ozone Cycloaddition

We accept the literature branching ratios reported by Zhang and Zhang for the first step of the mechanism, 0.59 addition at the 1,2 alkene (TS12) and 0.41 addition at the 3,4 alkene (TS34).^{6,7} This ratio is expected when considering the trend in [4+2] cycloaddition to dienes; alkenes with electron donating groups like the methyl group present at the 2 position of isoprene are more likely to undergo cycloaddition than an unsubstituted neighbor. Using CBS-QB3, we found that the best way to treat the cycloaddition was by treating ozone, isoprene, TS12, and TS34 as open-shelled singlets. Their $\langle S^2 \rangle$ values are 0.4081, 0.0000, 0.0000, and 0.0000 respectively at the B3LYP/6-311G(2d,d,p) level and 0.3962, 0.3283, 1.4436, and 1.4194 respectively at the UHF/CBSB3 level. Our results suggest that TS34 is 0.7 kcal/mole more favorable than TS12. This is contrary to expected and could be considered faulty. Since the reactants are starting at thermal equilibrium, 0.7 kcal/mole difference in the activation barrier would favor TS34 by a substantial margin, and we have already accepted the contrary to be true. We are unable to designate the origin of this faulty result but are not so interested because we have accepted the literature value, did not perform a variational transition state analysis, and have adopted the CBS-QB3 method to accurately predict the chemistry of the smaller, subsequent species.

D. Summary of Branching Ratios, Energetics, and Product Yields

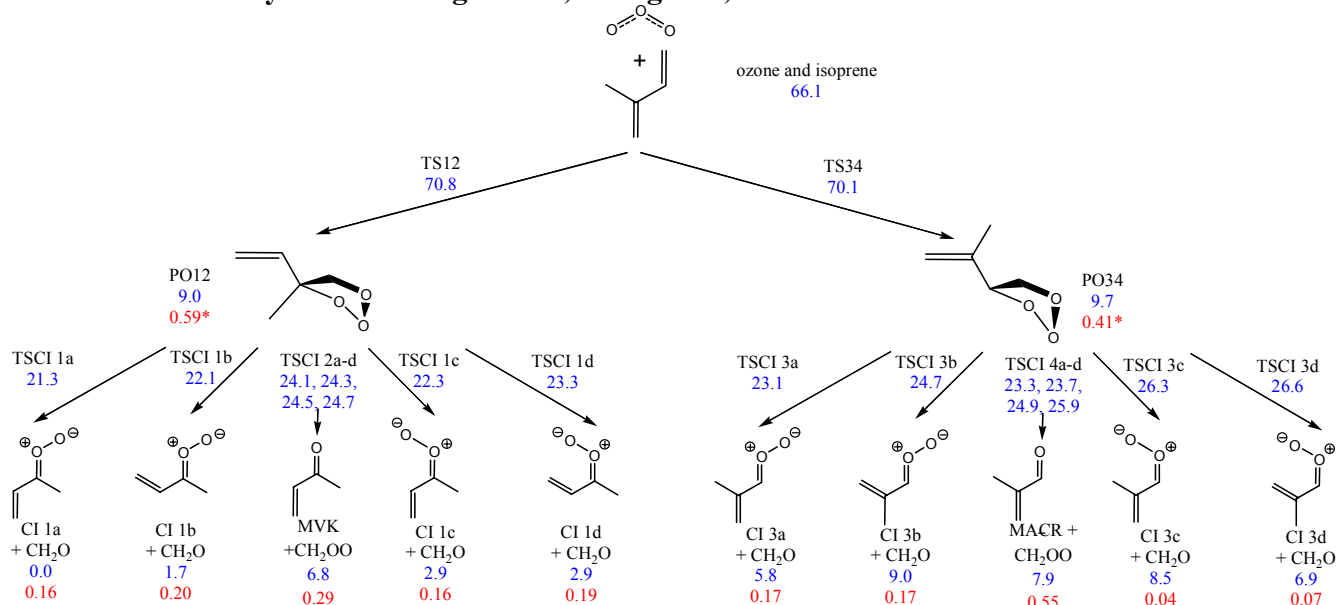


Figure 8. Schematic representing the cycloaddition and cycloreversion steps of ozonolysis observed. Blue numbers are CBS-QB3 zero-point corrected relative energies with respect to CI 1a, the most stable of the Criegee Intermediates. Red numbers are predicted branching ratios of master equation RRKM simulations. Branching ratios represent activated Criegee Intermediate formation and sum to one on each half of the Figure. * We have accepted *Zhang et al.*'s branching ratios for the cycloaddition step.⁶ Appendices A1-A5 have corresponding structures and bond lengths reported.

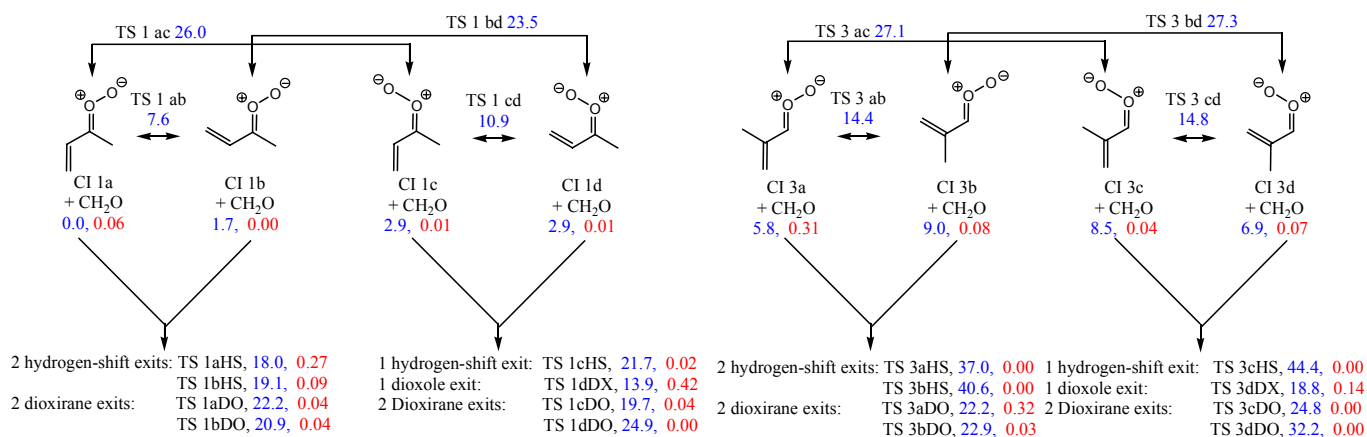


Figure 9. Schematic representing the interconversion and isomerization reactions of the eight substituted Criegee Intermediates. Isomerization reactions are grouped according to energy barriers; barriers of vinyl rotation are low enough that the Curtin-Hammett principle can be invoked. Blue numbers are CBS-QB3 zero-point corrected relative energies with respect to CI 1a, the most stable of the Criegee Intermediates. Red numbers are predicted branching ratios of master equation RRKM simulations; branching ratios sum to one for each half of the Figure, and here, thermalized Criegee Intermediate's ratios are reported. Figure 10 reports corresponding structures to those missing in this Figure. Appendices A4-A7 have corresponding structures and bond lengths reported.

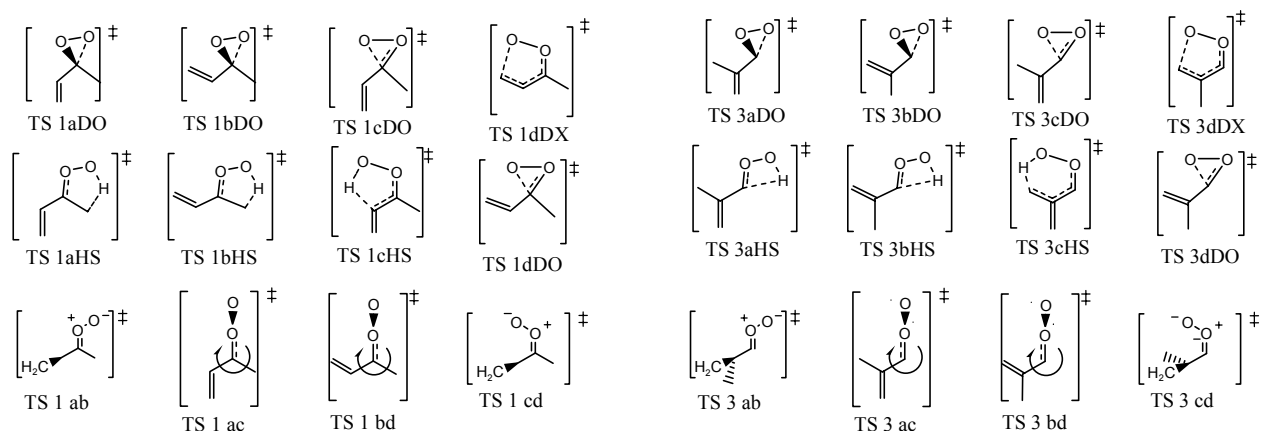


Figure 10. Corresponding transition structures to those missing from Figure 9. For bond lengths and more graphical structural depiction of these transition structures and their products look to appendices A4-A9.

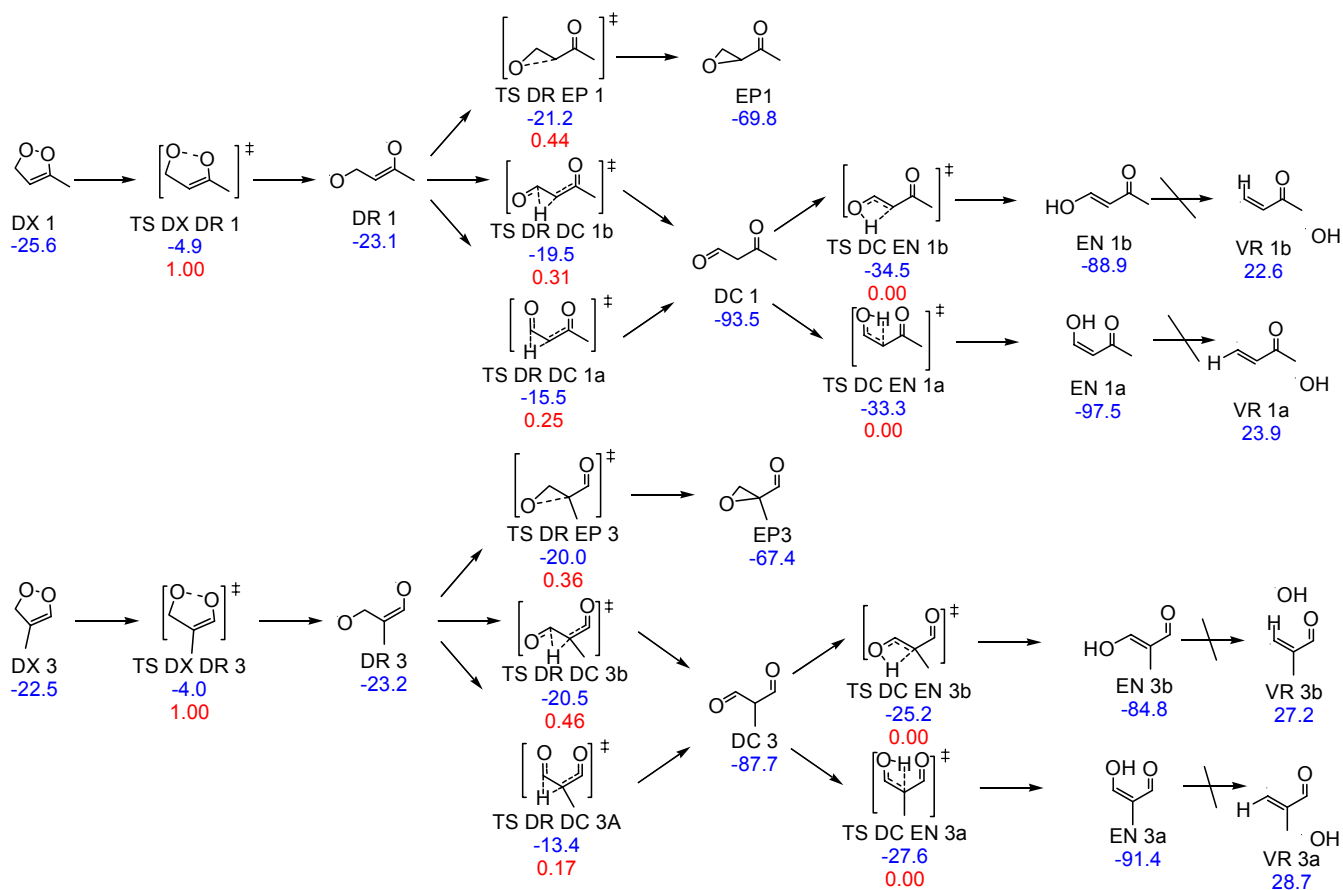


Figure 11. Summary of dioxole chemistry. Blue numbers are CBS-QB3 zero-point corrected relative energies with respect to CI 1a, the most stable of the Criegee Intermediates. Red numbers are predicted branching ratios of master equation RRKM simulations. Branching ratios equal one or zero for each set of transition states, so reaction is assumed to be complete or non-existent.

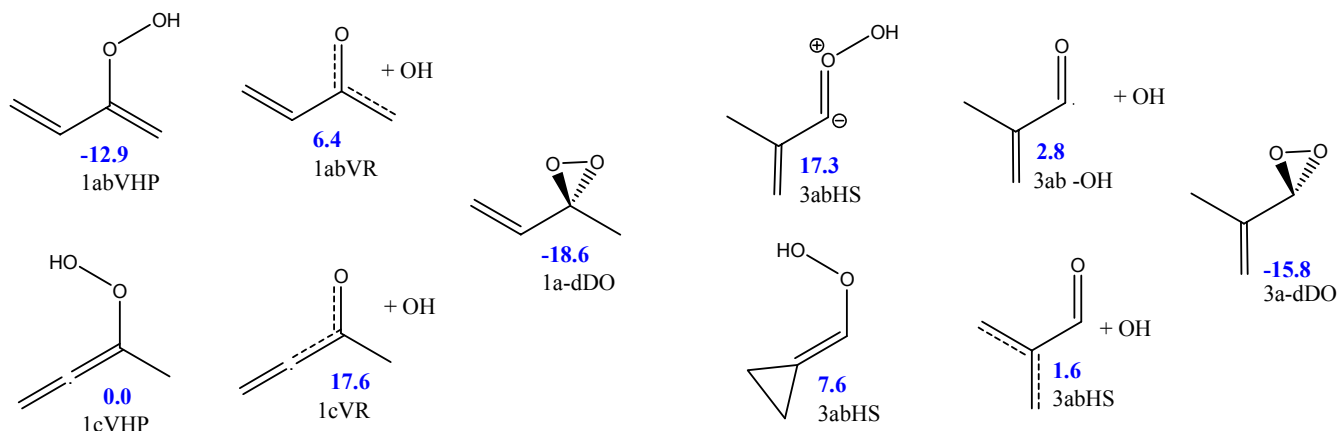


Figure 12. Summary of subsequent dioxirane formation and hydrogen shift intermediates. Blue numbers are CBS-QB3 zero-point corrected relative energies with respect to CI 1a, the most stable of the Criegee Intermediates. If more than one Criegee Intermediates converge to one product, only the lowest energy conformer of the product is shown here.

Figures 8-12 and Table 1 summarize the results of this report. There are several conclusions that can be derived from these results revealing information on structure, reactivity, and key products.

E. Stable Product Comparison with Experiment and Previous Theoretical work

In comparing our predictions of stable mechanistic products with observed values, the validity of our theory can be tested. We predict final yields for MACR, MVK, and formaldehyde of 0.23, 0.17, and 0.60 respectively. Earlier experimental work has observed yields of 0.32-0.42, 0.13-0.18, 0.86-0.96 for MACR, MVK and formaldehyde respectively^{6,50} Zhang *et al.* have previously predicted yields of 0.21, 0.12, and 0.67.⁶ Even correcting for reactions of isoprene with OH, observed results are prone to error, as is evident by the deviation from the expected sum of one for MACR, MVK and formaldehyde. Since we accept the literature branching ratios at the cycloaddition step, our predictions at this step do not dramatically differ with the previous prediction. Our results seem to better agree with experiment than previous predictions. We predict a slightly higher (MVK+MACR)/formaldehyde because CBS-QB3 reports a higher activation level and a smaller difference in the relative energies of cycloreversion transition barriers.

Table 1. Summary of absolute energies, reaction energies, 760 Torr branching ratios, and $\langle S^2 \rangle$ values

Species	CBS-QB3 Absolute Energy*	CCSD(T)/ 6- 31G(d) + CF** Absolute Energy	Preceding Species	Relative Energy w.r.t preceding species	Relative Energy w.r.t preceding species**	Branch Ratios	Branch Ratios**	Total percent Yield	Total Percent Yield**	$\langle S^2 \rangle$ UHF/ CBSB3
Attack at 1,2 alkene										
O ₃ + Isoprene	66.1	61.1	--							0.3962 (O ₃) 0.3283 (Is.)
TS12	70.8	64.4	O ₃ +Isoprene	4.7	3.3	0.59	0.59			1.4436
PO12	9.0	13.0	TS12	61.8	51.4					0.0000
Cycloreversion barriers and Criegee Intermediate Products										
TS Cl1a	21.3	24.3	PO12	12.3	11.3	0.16	0.44 for TS Cl 1a,b combined	0.03	0.14	0.0000
Cl 1a	0.0	0.0	TS Cl1a	-21.3	-24.3					0.0000
TS Cl1b	22.1	24.9	PO12	13.1	11.9	0.20				0.0000
Cl 1b	1.7	1.4	TS Cl1b	-20.4	-23.5					0.0000
TS Cl1c	22.3	25.3	PO12	13.3	12.3	0.16	0.35 for TS Cl 1c,d combined		0.07	0.0000
Cl 1c	2.9	2.5	TS Cl1c	-19.4	-22.8					0.0000
TS Cl1d	23.3	26.1	PO12	14.3	13.1	0.19				0.0000
Cl 1d	2.9	2.7	TS Cl1d	-20.4	-23.4					0.0000
TS Cl2a	24.1	27.0	PO12	15.1	14.0	0.07				0.0000
TS Cl2b	24.3	--	PO12	15.3	--	0.09	0.21 for TS Cl 2a-d combined			0.0000
TS Cl2c	24.5	--	PO12	15.5	--	0.08				0.0000
TS Cl2d	24.7	--	PO12	15.7	--	0.06				0.0000
MVK + Formyl Oxide	6.8	5.9	TS Cl 2a-d	[-17.3,-17.9]				0.17	0.12	0.0000
i) MVKox interconversion and exit channels										
TS 1 ab	7.6	--	Cl 1a,b	[7.6, 5.9]	--		0.08 are stabilized as Cl 1a		0.30 are stabilized as Cl 1a or b and 0.15 for Cl 1 c or d	0.0000
TS 1 ac	26.0	--	Cl 1a,c	[26.0, 23.1]	--					1.2142
TS 1 bd	23.5	--	Cl 1b,d	[21.8, 20.6]	--					1.2151
TS 1 cd	10.9	--	Cl 1c,d	[8.0, 8.0]	--					0.0000
TS 1aHS	18.0	18.8	Cl 1a	18.0	18.8	0.27		0.21		0.0000
TS 1bHS	19.1	19.8	Cl 1b	-17.4	-18.4	0.09				0.0000
1abVHP	-12.9	-15.0	TS 1a,bHS	[-30.9, -32.0]	[-33.8, -34.8]					0.0000
1abVR+OH	6.4	6.0	1abVHP	19.3	21.0			0.15	0.10	0.7671
TS 1cHS	21.7	24.4	Cl 1c	18.8	21.9	0.02	0.03			0.0000
1cVHP	0.0	-0.8	TS 1cHS	-21.7	-25.2					0.0000
1cVR+OH	17.6	11.5	1cVHP	17.6	12.3			0.01	0.01	0.7683
TS 1aDO	22.2	22.1	Cl 1a	22.2	22.1	0.04	0.04			0.0000
TS 1bDO	20.9	20.9	Cl 1b	19.2	19.5	0.04				0.0000
TS 1cDO	19.7	20.0	Cl 1c	16.8	17.5	0.04	0.27			0.0000
TS 1dDO	24.9	24.9	Cl 1d	22.0	22.2	0.00				0.0000
1a-dDO	-18.6	-18.2	TS 1a-dDO	[-38.3, -43.5]	[-38.2, -43.1]			0.05	0.14	0.0000
TS 1dDX	13.9	--	Cl 1d	11.0	--	0.42				0.0000
Dioxole Exit and subsequent pathway										
DX 1	-25.6	--	TS 1dDX	-39.5	--					0.0000
TS DX DR 1	-4.9	--	DX 1	20.7	--	1.00				1.1923
DR 1	-23.1	--	TS DX DR 1	-18.2	--					1.1227
TS DR EP 1	-21.2	--	DR 1	1.9	--	0.44				1.1156
EP 1	-69.8	--	TS DR EP 1	-48.6	--			0.08		0.0000
TS DR DC 1a	-15.5	--	DR 1	7.6	--	0.25				1.0785
TS DR DC 1b	-19.5	--	DR 1	3.6	--	0.31				1.0647
DC 1	-93.5	--	TS DR DC 1a,b	[-74.0, -78.0]	--			0.10		0.0000
TS DC EN 1a	-33.3	--	DC 1	60.2	--	0.00				0.0000
EN 1a	-97.5	--	TS DC EN 1a	-64.2	--					0.0000
TS DC EN 1b	-34.5	--	DC 1	59.0	--	0.00				0.0000
EN 1b	-88.9	--	TS DC EN 1b	-54.4	--					0.0000
VR 1a	23.9	--	EN 1a	121.4	--					1.0565
VR 1b	22.6	--	EN 1b	111.5	--					1.0477

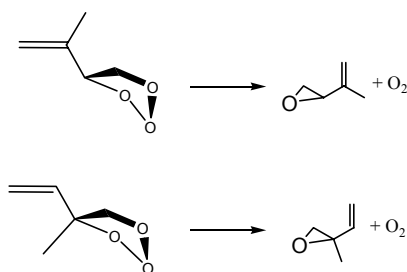
Species	CBS-QB3 Absolute Energy*	CCSD(T)/ 6- 31G(d) + CF** Absolute Energy	Preceding Species	Relative Energy w.r.t preceding species	Relative Energy w.r.t preceding species**	Branch Ratios	Branch Ratios**	Total percent Yield	Total Percent Yield**	<S ² > UHF/ CBSB3
Attack at 3,4 alkene										
O ₃ +Isoprene	66.1	61.1								0.3962 (O ₃)
TS34	70.1	64.5	O ₃ +Isoprene	4.0	3.4	0.41	0.41			0.3283 (Is.)
PO34	9.7	13.8	TS34	60.4	50.7					1.4194
										0.0000
Cycloreversion barriers and Criegee Intermediate Products										
TS Cl3a	23.1	26.1	PO34	13.4	12.3	0.17				0.0000
Cl 3a	5.8	5.0	TS Cl3a	-17.3	-21.1		0.44 for TS Cl 3a,b combined	0.06	0.04	0.0000
TS Cl3b	24.7	27.5	PO34	15.0	13.7	0.17				0.0000
Cl 3b	9.0	7.9	TS Cl3b	-15.7	-19.6			0.01		0.0000
TS Cl3c	26.3	29.4	PO34	16.6	15.6	0.04	0.05 for TS Cl 3c,d combined	0.01	0.01	0.0000
Cl 3c	8.5	8.1	TS Cl3c	-17.8	-21.3			0.01	0.01	0.0000
TS Cl3d	26.6	29.7	PO34	16.9	15.9	0.07				0.0000
Cl 3d	6.9	6.7	TS Cl3d	-19.7	-23.0			0.01		0.0000
TS Cl4a	23.3	26.0	PO34	13.6	12.2	0.18				0.0000
TS Cl4b	23.7	--	PO34	14.0	--	0.16	0.51 for TS Cl 4a-d combined			0.0000
TS Cl4c	24.9	--	PO34	15.2	--	0.11				0.0000
TS Cl4d	25.9	--	PO34	16.2	--	0.10				0.0000
MACR + Formyl Oxide	7.9	7.0	TS Cl 4a-d	[-15.4,-18.0]				0.23	0.21	0.0000
MACRox interconversion barriers and exit channels										
TS 3 ab	14.4	--	Cl 3a,b	[8.6, 5.4]	--	Stabilization of Cl 1a-d of 0.31, 0.08, 0.04, and 0.07 respectively	0.18 are stabilized as Cl 3a or b and 0.04 for Cl 1 c or d			0.0000
TS 3 ac	27.1	--	Cl 3a,c	[21.3, 18.6]	--					1.2185
TS 3 bd	27.3	--	Cl 3b,d	[18.3, 20.4]	--					1.2196
TS 3 cd	14.8	--	Cl 3c,d	[6.3, 7.9]	--					0.0000
TS 3aHS	37.0	36.2	Cl 3a	31.2	31.2	0.00	0.00			0.0000
TS 3bHS	40.6	39.5	Cl 3b	-31.6	-31.6	0.00				0.0000
3abHS	17.3	14.4	TS 3a,bHS	[-19.7, -23.3]	[-21.8, -25.1]					0.0000
3ab-OH	2.8	-8.1	3abHS	-14.5	-22.5					0.8438
TS 3cHS	44.4	44.3	Cl 3c	35.9	36.2	0.00	0.00			0.0000
3cHS	7.6	7.3	TS 3cHS	-36.8	-37.0					0.0000
3cHS-OH	1.6	-6.7	3cHS	-6.0	-14.0					0.7857
TS 3aDO	22.2	21.7	Cl 3a	16.4	16.7	0.32				0.0000
TS 3bDO	22.9	22.4	Cl 3b	13.9	14.5	0.03	0.72			0.0000
TS 3cDO	24.8	25.0	Cl 3c	16.3	16.9	0.00	0.06			0.0000
TS 3dDO	32.2	32.2	Cl 3d	25.3	25.5	0.00				0.0000
3a-dDO	-15.8	-15.5	TS 3a-dDO	[-38.0, -48.0]	[-40.5, -47.7]			0.06	0.16	0.0000
TS 3dDX	18.8	--	Cl 3d	11.9	--	0.14				0.0000
Dioxole Exit and subsequent pathway										
DX 3	-22.5	--	TS 3dDX	-41.3	--					0.0000
TS DX DR 3	-4.0	--	DX 3	18.5	--	1.00				1.1734
DR 3	-23.2	--	TS DX DR 3	-19.2	--					1.1339
TS DR EP 3	-20.0	--	DR 3	3.2	--					1.1377
EP 3	-67.4	--	TS DR EP 3	-47.4	--			0.01		0.0000
TS DR DC 3a	-13.4	--	DR 3	9.8	--	0.17				1.0949
TS DR DC 3b	-20.5	--	DR 3	2.7	--	0.46				1.0723
DC 3	-87.7	--	TS DR DC 3a,b	[-74.3, -67.2]	--			0.02		0.0000
TS DC EN 3a	-27.6	--	DC 3	60.1	--	0.00				0.0000
EN 3a	-91.4	--	TS DC EN 3a	-63.8	--					0.0000
TS DC EN 3b	-25.2	--	DC 3	62.5	--	0.00				0.0000
EN 3b	-84.8	--	TS DC EN 3b	-59.6	--					0.0000
VR 3a	28.7	--	EN 3a	120.1	--					0.7636
VR 3b	27.2	--	EN 3b	112.0	--					0.7632

* Absolute energies are calculated zero-point corrected energies with respect to Cl 1a, the lowest energy Criegee Intermediate.
**Branching ratios and Zero-point corrected energies that come from previous quantum mechanic and kinetic studies of Zhang et al.^{6,7} Branching ratios reported sum to one for each mechanistic step while total yields combine all branching ratios to make a final prediction for the scope of this study.

F. Theoretical discovery of oxoepoxides

To evaluate the predictive powers of the third mechanistic step, the Criegee Intermediate isomerization reaction, observed OH yields, dioxirane yields, epoxide yields, dicarbonyl yields and dioxirane yields would be appropriate. Currently, only experimental OH-yield and structurally analogous epoxide yields have been reported.

The epoxides we predict to be present, 1,2-epoxy-3-oxobutane and 1,2-epoxy-2-methyl-3-oxopropane, are shown as EP 1 and EP 3 in Figure 11 above. Epoxides have been shown to form as a result of isoprene ozonolysis, but EP 1 and EP 3 were not reported. It was once believed that primary ozonides could decompose to form molecular oxygen and epoxides with a vinyl group in place of the oxo groups of EP 1 and EP 3 instead of undergoing cycloreversion as shown in Scheme 6.⁵¹



The observed yield of these two alkenyl epoxides are non-negligible at 0.053.⁵¹ The decomposition shown in Scheme 6 has not gained acceptance, but present results indicate that the structurally similar EP 1 and EP 3 may have been confused in such experimental analyses. We predict yields of 0.08 and 0.01 for EP 1 and EP 3 respectively, which are contrary to the relative yields of epoxides in Scheme 6 refuting our conclusion.⁵¹

G. OH yield prediction and analysis

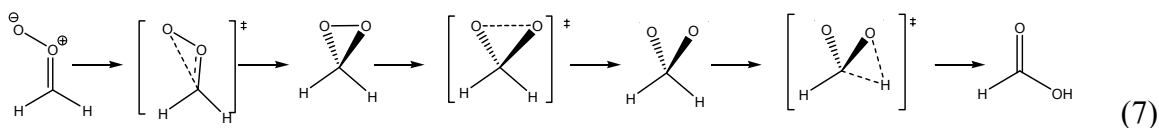
i. Prediction and comparison to previous results

OH-yield has been extensively studied for this system. OH-yields from isoprene ozonolysis vary widely but are much more reliable than results for some alkenes; eight reported values range from 0.19 to 0.53, with all but two results between 0.19 and 0.27.⁶ Past theoretical work predicts a ‘prompt’ yield of 0.11 and a ‘thermal’ yield of 0.14

meaning that stabilized Criegee intermediates will eventually react to form OH, which is debated in the literature.⁶ Our prediction of 0.16 at 1 atm is significantly lower than the experimentally observed values; however, our predictions do not include uncertain OH sources.

ii. Uncertain sources of OH radical

The following are possible additional sources of OH that our predictions do not consider. Ethene ozonolysis is known to produce OH, which some believe to be through the bond cleavage of a ‘hot’ formic acid intermediate as shown in Scheme 7.



Most experimental results give a OH-yield of around 0.10 for ethene ozonolysis, but its theoretical understanding is widely debated with Scheme 7 being just one possible explanation.⁵²⁻⁵⁸ We predict a formyl oxide yield of 0.40. The formyl oxide resulting from isoprene ozonolysis would be much less activated since MVK or MACR will absorb a majority of the energy released in primary ozonide decomposition probably leading to a much lower OH-yield than in ethene ozonolysis experiments.

The fate of thermalized substituted and unsubstituted Criegee intermediates has recently been debated in the literature^{52,53,59-61} with special attention to isoprene.^{59,60} Studies suggest that water will act as a reactive sink for the thermalized Criegee Intermediates forming primarily hydroxyalkyl hydroperoxides and should not be considered an OH source.^{59,60} This laboratory is currently beginning investigation into the importance of hydrogen tunneling in hydrogen-shift reactions eventually hoping to effectively model the fate of the thermalized Criegee Intermediate.

The Curtin-Hammett principle was invoked for master equation simulations of cycloreversion possibly affecting the relative yields of CI 1a-d,3a-d, CI 1a in particular, and eventual OH yields. Further investigation is needed to determine the possible effects

of this assumption. Because the K-rotor is assumed to be an internal degree of freedom transition structures can be highly entropically distinct from one another impacting reactivity greatly as a universal minimum is used when the Curtin-Hammett principle is invoked. If all minima and interconversion barriers are taken into account, the differences in the density of states of multiple reactants' states will more fully represent the differences in reaction barriers' entropy. For an example, Figure 8 demonstrates the relative energy and relative branching of the cycloreversion barriers; TS CI 1a is the most energetically favorable but least likely mode of reaction for TS CI 1a-d because of its more prolate structure and lower degree of rotational entropy. The overarching theory for this discrepancy is discussed with regards to equation 2 earlier in this report. By including all minima and barriers to conformer interconversion in the master equation simulations, the relative entropy of reaction barriers to their minima would be more adequately described giving a more accurate prediction of hydroxyl yield.

An analogous pathway to the formic acid pathway described in Scheme 7 is not possible for DO 1 and DO 3 because O-O bond cleavage is unlikely when energy is distributed over a greater range of vibrational degrees of freedom.

The possible additional sources of OH radical would most likely not be more than a few percent moving our prediction closer to experimental results, an improvement to the previous theoretical prediction of 0.11.⁶

iii. Pressure dependence of OH and other mechanistic intermediates

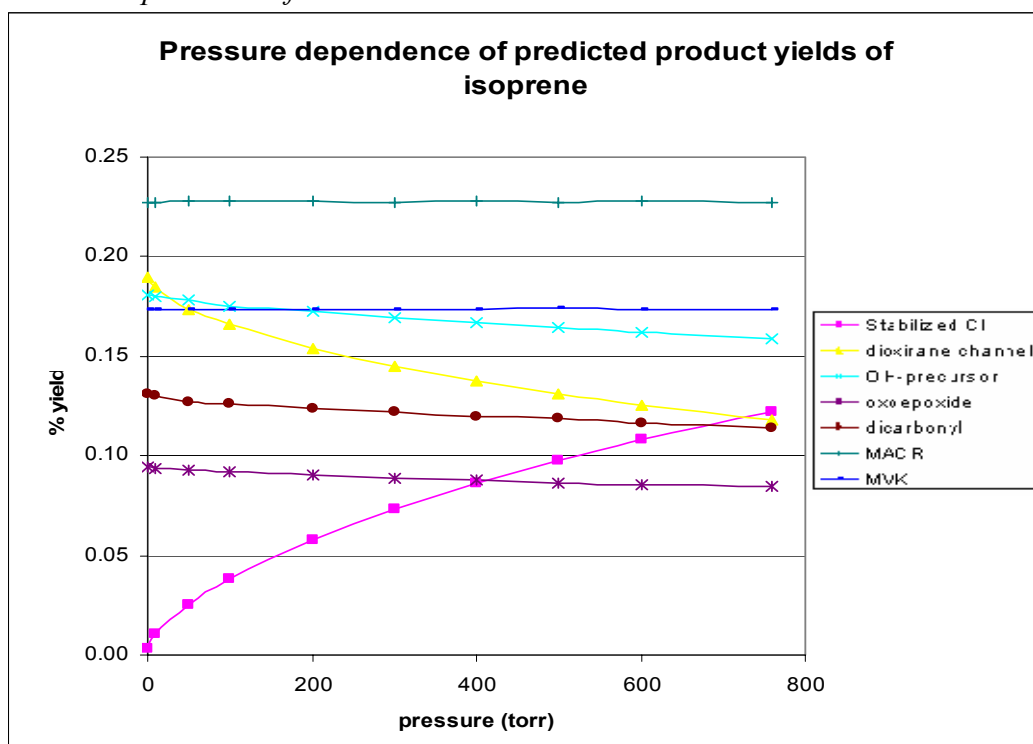


Figure 13. Summary of pressure dependence for final points of master equation simulations. Formyl oxide, not shown for clarity, can be represented by the sum of MACR and MVK, 0.40.

There is little pressure dependence in OH prediction as can be seen in Figure 13. As pressure increases, dioxirane formation is shown to be most affected by collisional stabilization dropping from 0.19 at 0 Torr to 0.12 at 760 Torr while OH forming channels only drop from 0.18 to 0.16 over the same pressure range. Stabilization increases from near 0.00 to ~0.13 from 0-760 Torr respectively. Collisional stabilization of Criegee Intermediates most affects dioxirane formation and has little effect on dioxole channels (oxoepoxide and dicarbonyl) and hydrogen-shift OH-precursor channels. Dioxirane formation is the only competitive reaction channel for CI 3a,b, the dominant forms of MACRox, and MACRox conformers are less activated than those of MVKox, which implies a strong competition between collisional stabilization and dioxirane formation, as is evident in Figure 13. Hydrogen-shift channels are only competitive for MVKox conformers, which have a low degree of collisional stabilization as shown in Table 1; because collisional stabilization is not very competitive for MVKox conformers'

hydrogen-shift channels show little pressure dependence. The same is true for dioxole formation because the branching ratios leading to CI 3c,d, from which dioxole formation is competitive, are very small as shown in Table 1. Dioxole formation is also the lowest reaction barrier making it less sensitive to stabilization competition in this system. While all reaction barriers are only slightly dependent upon pressure and collisional stabilization, dioxirane formation from MACRox and MVKox is very sensitive to pressure increase.

H. Stabilized Criegee Intermediate Yields

Comparing predicted yields of stabilized Criegee Intermediates can also help to compare this study with previous theoretical work on isoprene ozonolysis. Table 1 offers the best comparison tool. This study predicts a yield of 0.03 for CI 1a and 0 for CI 1b-d while previous work predicts 0.14. Stabilized MACRox yields are 0.06, 0.01, 0.01, and 0.01 for CI 3a-d respectively as compared to previous work that predicts 0.04 for CI 3a,b combined and 0.01 for CI 3c,d combined. Dramatically higher stabilization yields for CI 1a-d in previous studies can be explained. For explanation, in this study, Criegee Intermediates are more vibrationally activated increasing the chance of reaction versus stabilization, and the dioxole-forming channel increases the probability of reaction for CI 1c,d.

For CI 3a-d, comparison of branching ratios predicts an opposite trend to that shown for CI 1a-d. As seen in Table 1, the previous work predicts stabilization yields of 0.18 for CI 3a,b and 0.04 for CI 3c,d while this study predicts 0.31, 0.08, 0.04, and 0.07 for CI 3a-d respectively meaning that this study is predicting over two times as much stabilization as previous work. In considering the greater activation of Criegee Intermediates in this study, and the already compared branching ratios for CI 1a-d, these results are troubling. Because MACRox and respective transition states are ~ 5 kcal/mole higher than those for MVKox, the MACRox pathway is less activated making collisional

stabilization more important and likely shown by the dramatic increase of collisional stabilization branching for this study in Table 1. The same trend should hold true for the previous study, but in fact, the amount of collisional stabilization decreases for CI 3a-d as compared to CI 1a-d. There are several possible causes for this difference that could be explained by any combination of the differences in method such as the average collisional stabilization energy $\langle \Delta E \rangle$, treatment of interconversion, and exit channel energies.

I. Hydrogen-shift versus Dioxirane formation: Resonance Arguments

Quantum chemical results explain very simple resonance stabilization effects.

When looking at three different *syn*-methylcarbonyl oxides with differing amounts of substitution in Figure 14, the difference in hydrogen-shift and dioxirane closure barriers decreases as the carbonyl oxide becomes more stable.

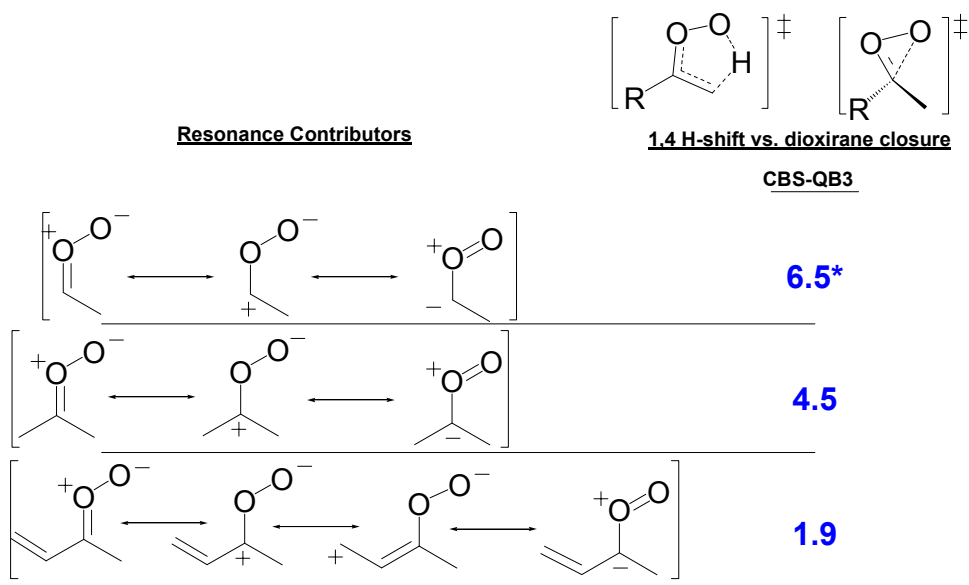


Figure 14. The competition of dioxirane formation and 1,4 hydrogen shift are shown for a variety of substituted methyl carbonyl oxides. Blue numbers are the differences of CBS-QB3 zero-point corrected relative energies with the hydrogen shift being more stable in each case. *Results from previous studies^{26,62}

Dioxirane formation results from the Criegee Intermediate resonance contributor that puts the positive charge at the carbonyl carbon and the negative charge at the terminal oxygen. As stabilization of the carbocationic character increases, CBS-QB3 predicts that dioxirane formation will be more competitive with 1,4 hydrogen shift. The

third resonance contributor of the methyl vinyl substituted carbonyl oxide shows how the *syn*-vinyl conformer could readily close to form a five-membered ring.

Conclusions

This study applies the most accurate quantum chemical model to isoprene ozonolysis to date and explores previously undiscovered dioxole-formation and subsequent pathways. Ozone-isoprene cycloaddition, primary ozonides, cycloreversion, Criegee Intermediates, dioxirane formation and hydrogen-shifts, which have already been described theoretically, have been more accurately described using CBS-QB3 composite method chemistry while six formyl oxide-forming cycloreversion barriers, Criegee intermediate interconversion barriers, and dioxole chemistry have been explored for the first time. Energetically, this study shows similar trends with the previous investigation supporting both theories, and this study kinetically predicts a ‘prompt’ OH-yield more consistent with experiment than the previous study.

The presence of oxoepoxides and dicarbonyls has been explained as result of dioxole chemistry. Further experimental work should attempt to find these species’ concentrations in hopes of determining the importance of the dioxole channel. These data should give insight into the branching ratios at the cycloreversion step.

There are several steps to take in improving results. They include in-depth variational transition state analysis of the cycloaddition step, improving collisional stabilization models and parameters, and full treatment of primary ozonide conformers and interconversion barriers.

Acknowledgements

I would like to first and foremost thank Professor Kuwata for all of his help and patience with me. For funding, I would like to thank the Beltmann Fund and the ACS Petroleum Research Fund. I would also like to give a big thanks to my parents, brothers, Macalester College, the faculty of the chemistry department, and the student research community.

Works Cited

- (1) Thompson, A. M. *Science* **1992**, *256*, 1157.
- (2) Hu, J.; Stedman, D. H. *Environ. Sci. Technol.* **1995**, *29*, 1655.
- (3) Heard, D. E.; Pilling, M. J. *Chem. Rev.* **2003**, *103*, 5163.
- (4) Guenther, A.; Hewitt, C. N.; Erickson, D.; Fall, R.; Geron, C.; Graedel, T.; Harley, P.; Klinger, L.; Lerdau, M.; McKay, W. A.; Pierce, T.; Scholes, B.; Steinbrecher, R.; Tallamraju, R.; Taylor, J.; Zimmerman, P. *J. Geophys. Res.* **1995**, *100*, 8873.
- (5) Faloon, I.; Tan, D.; Brune, W.; Hurst, J.; Barkot, D.; Couch, T. L.; Shepson, P.; Apel, E.; Riemer, D.; Thornberry, T.; Carroll, M. A.; Sillman, S. K., G. J.; Sagady, J.; Hooper, D.; Paterson, K. *JOURNAL OF GEOPHYSICAL RESEARCH-ATMOSPHERES* **2001**, *106*, 24315.
- (6) Zhang, D.; Lei, W.; Zhang, R. *Chem. Phys. Lett.* **2002**, *358*, 171.
- (7) Zhang, D.; Zhang, R. *J. Am. Chem. Soc.* **2002**, *124*, 2692.
- (8) Foresman, J. B.; Frisch, A. *Exploring Chemistry with Electronic Structure Methods*, Second ed.; Gaussian Inc.: Pittsburgh, PA, 1993, 1995-96.
- (9) Forst, W. *Theory of Unimolecular Reactions*; Academic Press: New York, 1972.
- (10) Holbrook, K. A.; Pilling, M. J.; Robertson, S. *Unimolecular Reactions*; Wiley: New York, 1996.
- (11) Barker, J. R. *Intl. J. Chem. Kinet.* **2001**, *33*, 232.
- (12) Kroll, J. H.; Sahay, S. R.; Anderson, J. G.; Demerjian, K. L.; Donahue, N. *M. J. Phys. Chem. A* **2001**, *105*, 4446.
- (13) Olzmann, M.; Kraka, E.; Cremer, D.; Gutbrod, R.; Andersson, S. *J. Phys. Chem. A* **1997**, *101*, 9421.
- (14) Mourits, F. M.; Rummens, F. H. A. *Can. J. Chem.* **1977**, *55*, 3007.
- (15) Hippler, H.; Troe, J.; Wendelken, H. *J. Chem. Phys.* **1983**, *78*, 6709.

- (16) Hirschfelder, J. O.; Curtiss, C. F.; Bird, R. B. *Molecular Theory of Gases and Liquids*; Wiley: New York, 1954.
- (17) Becke, A. D. *J. Chem. Phys.* **1993**, *98*, 5648.
- (18) Stephens, P. J.; Devlin, F. J.; Chabalowski, C. F.; Frisch, M. J. *J. Phys. Chem.* **1994**, *98*, 11623.
- (19) Hehre, W. J.; Ditchfield, R.; Pople, J. A. *J. Chem. Phys.* **1972**, *56*, 2257.
- (20) Hariharan, P. C.; Pople, J. A. *Theoret. Chim. Acta.* **1973**, *28*, 213.
- (21) Gonzalez, C.; Schlegel, H. B. *J. Chem. Phys.* **1989**, *90*, 2154.
- (22) Gonzalez, C.; Schlegel, H. B. *J. Phys. Chem.* **1990**, *94*, 5523
- (23) Gutbrod, R.; Kraka, E.; Schindler, R. N.; Cremer, D. *J. Am. Chem. Soc.* **1997**, *119*, 7330.
- (24) Gutbrod, R.; Schindler, R. N.; Kraka, E.; Cremer, D. *Chem. Phys. Lett.* **1996**, *252*, 221.
- (25) Fenske, J. D.; Kuwata, K. T.; Houk, K. N.; Paulson, S. E. *J. Phys. Chem. A* **2000**, *104*, 7246.
- (26) Kuwata, K. T.; Templeton, K. L.; Hasson, A. S. *J. Phys. Chem. A* **2003**, *107*, 11525.
- (27) Fenske, J. D.; Hasson, A. S.; Paulson, S. E.; Kuwata, K. T.; Ho, A.; Houk, K. N. *J. Phys. Chem. A* **2000**, *104*, 7821.
- (28) Cremer, D.; Kraka, E.; Szalay, P. G. *Chem. Phys. Lett.* **1998**, *292*, 97.
- (29) Coote, M. L. *J. Phys. Chem. A* **2004**, *108*, 3865
- (30) Lynch, B. J.; Fast, P. L.; Harris, M.; Truhlar, D. G. *J. Phys. Chem. A* **2000**, *104*, 4811.
- (31) Lynch, B. J.; Truhlar, D. G. *J. Phys. Chem. A* **2001**, *105*, 2936.
- (32) Jursic, B. S. *J. Mol. Struct. Theochem.* **1998**, *430*, 17.

- (33) Malick, D. K.; Petersson, G. A.; Montgomery, J. A., Jr. *J. Chem. Phys.* **1998**, *108*, 5704.
- (34) Zhao, Y.; Pu, J.; Lynch, B. J.; Truhlar, D. G. *Phys. Chem. Chem. Phys.* **2004**, *6*, 673.
- (35) Montgomery, J. A., Jr.; Frisch, M. J.; Ochterski, J. W.; Petersson, G. A. *J. Chem. Phys.* **1999**, *110*, 2822.
- (36) Gomez-Balderas, R.; Coote, M. L.; Henry, D. J.; Radom, L. *J. Phys. Chem. A* **2004**, *108*, 2874.
- (37) Henry, D. J.; Parkinson, C. J.; Radom, L. *J. Phys. Chem. A* **2002**, *106*, 7927.
- (38) Guner, V.; Khuong, K. S.; Leach, A. G.; Lee, P. S.; Bartberger, M. D.; Houk, K. N. *J. Phys. Chem. A* **2003**, *107*, 11445.
- (39) Parkinson, C. J.; Mayer, P. M.; Radom, L. *Theor. Chem. Acc.* **1999**, *102*, 92.
- (40) Ochterski, J. W.; Petersson, G. A.; Montgomery, J. A., Jr. *J. Chem. Phys.* **1996**, *104*, 2598.
- (41) Bartlett, R. J. *J. Phys. Chem.* **1989**, *93*, 1697.
- (42) Barker, J. R. MultiWell; 1.3.2 ed.; University of Michigan: Ann Arbor, MI, July 2003.
- (43) Barker, J. R.; Ortiz, N. F. *Intl. J. Chem. Kinet.* **2001**, *33*, 246.
- (44) Houston, P. L. *Chemical Kinetics and Reaction Dynamics*, 1st ed.; McGraw-Hill: New York, 2001.
- (45) *Lange's Handbook of Chemistry*, Fourteenth ed.; McGraw-Hill: New York, 1992.
- (46) McCann, D. W.; Danner, R. P. *Ind. Engr. Chem. Process Des. Dev.* **1984**, *23*, 529.

- (47) Reid, R. C.; Prausnitz, J. M.; Poling, B. E. *The Properties of Gases and Liquids*, Fourth ed.; McGraw-Hill: New York, 1987.
- (48) Joback, K. G.; Reid, R. C. *Chem. Engr. Commun.* **1987**, *57*, 233.
- (49) Barker, J. R.; Yoder, L. M.; King, K. D. *J. Phys. Chem. A* **2001**, *105*, 796.
- (50) Atkinson, R.; Aschmann, S. M. *Environ. Sci. Technol.* **1994**, *28*, 1539.
- (51) Atkinson, R.; Aschmann, S. M.; Arey, J.; Tuazon, E. C. *Res. Chem. Intermed.* **1994**, *20*, 385.
- (52) Ryzhkov, A. B.; Ariya, P. A. *Phys. Chem. Chem. Phys.* **2004**, *21*, 5042.
- (53) Hasson, A. S.; Chung, M. Y.; Kuwata, K. T.; Converse, A. D.; Krohn, D.; Paulson, S. E. *J. Phys. Chem. A* **2003**, *107*, 6176.
- (54) Kroll, J. H.; Donahue, N. M.; Cee, V. J.; Demerjian, K. L.; Anderson, J. G. *J. Am. Chem. Soc.* **2002**, *124*, 8518.
- (55) Anglada, J. M.; Crehuet, R.; Bofill, J. M. *Chem. Eur. J.* **1999**, *5*, 1809.
- (56) Aplincourt, P.; Ruiz- López, M. F. *J. Phys. Chem. A* **2000**, *104*, 380.
- (57) Hasson, A. S.; Ho, A. W.; Kuwata, K. T.; Paulson, S. E. *J. Geophys. Res.* **2001**, *106*, 34143.
- (58) Kroll, J. H.; Hanisco, T. F.; Donahue, N. M.; Demerjian, K. L.; Anderson, J. G. *J. Geophys. Res. Lett.* **2001**, *28*, 3863.
- (59) Aplincourt, P.; Anglada, J. M. *J. Phys. Chem.* **2003**, *107*, 5798.
- (60) Aplincourt, P.; Anglada, J. M. *J. Phys. Chem.* **2003**, *107*, 5812.
- (61) Ryzhkov, A. B.; Ariya, P. A. *Chem. Phys. Lett.* **2003**, *367*, 423.
- (62) Kuwata, K. T.; Hasson, A. S.; Dickinson, R. V.; Petersen, E. B.; Valin, L. *C. J. Phys. Chem.* **2005**, *109*, 2514.

Appendices